Journal of Power Sources 196 (2011) 9939–9945

Contents lists available at SciVerse ScienceDirect

Journal of Power Sources

journal homepage: www.elsevier.com/locate/jpowsour

Performance of $LaBaCo_2O_{5+\delta}$-Ag with B_2O_3-Bi_2O_3-PbO frit composite cathodes for intermediate-temperature solid oxide fuel cells

Ruifeng Li, Lei Gao, Lin Ge, Yifeng Zheng, Ming Zhou, Han Chen, Lucun Guo*

College of Materials Science and Engineering, Nanjing University of Technology, No. 5 Xinmofan Road, Nanjing, Jiangsu 210009, PR China

ARTICLE INFO

Article history:
Received 10 April 2011
Received in revised form 17 May 2011
Accepted 3 June 2011
Available online 26 August 2011

Keywords:
Cathode-Ag
B_2O_3-Bi_2O_3-PbO frit
Thermal expansion
Electrical conductivity
Electrochemical performance

ABSTRACT

The composite cathodes $LaBaCo_2O_{5+\delta}$-*x* wt.% Ag (LBCO-*x*Ag, *x* = 20, 30, 40, 50) were prepared by mechanical mixing method for intermediate-temperature solid oxide fuel cells (IT-SOFCs). The experiment results indicated that the addition of a small amount of B_2O_3-Bi_2O_3-PbO (BBP) frit to LBCO-*x*Ag can effectively improve the adhesion and strength of cathode membrane without damaging its porous structure. The BBP frit was proved effective for lowering the sintering temperature of LBCO-*x*Ag to 900 °C. According to the electrochemical impedance spectroscopy and cathodic polarization analysis, the LBCO-30Ag exhibited the best performance and the optimal BBP frit content was 2.5 wt.%. For LBCO-30Ag with 2.5 wt.% BBP frit, the area-specific resistance based on $Sm_{0.2}Ce_{0.8}O_{1.9}$ (SDC) electrolyte decreased by about 57.6% at 700 °C, 60.5% at 750 °C and 75.9% at 800 °C compared to LBCO, and its cathodic overpotential was 10.7 mV at a current density of 0.2 A cm^{-2} at 700 °C, while the corresponding value for LBCO was 51.0 mV. The addition of Ag and BBP frit to LBCO had no significant effect on the thermal expansion.

1. Introduction

Solid oxide fuel cells (SOFCs) are efficient and clean power generation devices, which can convert chemical energy of fuel into electrical energy directly [1–4]. Lowering their operating temperature to intermediate-temperature range of about 500–800 °C represents the research mainstream and has received widespread investigation recently. The lower operating temperature would solve various problems caused by the conventional SOFCs which operated at high temperature (~1000 °C), such as high fabrication cost, limited choice of materials and chemical reaction among the components [4,5]. However, when the operating temperature is decreased, the polarization resistance and overpotential of cathode will increase correspondingly, leading to a decreased electrocatalytic activity for the oxygen reduction reaction (ORR) [6–8]. Therefore, considerable effort should be spent on improving the electrochemical performance of cathode at lower temperature.

One effective strategy to improve the cathode performance at intermediate-temperature range is to modify the cathode with noble metals [9–16]. Ag is reported to be an attractive additive for cathode because it can improve the electronic conductivity, enhance the electrocatalytic properties for the oxygen reduction reaction and is more affordable than Pd, Pt, etc. [17–22]. Many cathode-Ag composite cathodes had been reported to be potential cathodes for IT-SOFCs. The area specific resistance (ASR) of $(BaO)_{0.11}(Bi_2O_3)_{0.89}$-50 vol.% Ag composite cathode was about 20 times lower than that of pure cathode at 650 °C [21]. The addition of 3 wt.% Ag to $Ba_{0.5}Sr_{0.5}Co_{0.8}Fe_{0.2}O_{3-\delta}$ resulted in about 54.5% reduction in the area specific resistance and 29.4% reduction in the activity energy (Ea) at 650 °C in air reported by Ye Lin et al. [22]. The infiltration of about 18 wt.% Ag into $La_{0.6}Sr_{0.4}Co_{0.2}Fe_{0.8}O_3$ cathode resulted in the enhancement of the power density of about 50% [17].

However, the preparation of cathode-Ag composite cathodes appears still to be a challenge. The low sintering temperature limited by the thermal evaporation [23] and low melting point of Ag (~962 °C) generally results in a weak interfacial adhesion between cathode-Ag and electrolyte, leading to a decreased electrochemical performance. Many methods have been exploited for the preparation of cathode-Ag electrodes, such as impregnation [8,14], electroless deposition [20,24,25], etc. All these methods, Ag was added after sintering of cathode and then sintered the cathode-Ag at a relatively low temperature to avoid the melting of Ag and reduce the Ag thermal evaporation. However, there still remain many problems to be solved: the amount of Ag loaded by the impregnation method is limited [8,19], the adhesion between Ag precursor and the ceramic matrices is weak [14] and the thermal decomposition of the Ag precursor would form severe pore to damage the cathode functional layer (CFL) [16]. The electroless deposition are not suitable for modifying the cathode containing Ba and/or Sr ions with Ag because the reducing agents in this method could lead to the formation of carbonates ($Ba_xSr_{1-x}CO_3$) which not only occupy the active sites for ORR, but also block the oxygen adsorption and surface diffusion [20,25]. In addition, for the

* Corresponding author. Tel.: +86 25 83587261; fax: +86 25 83306152.
E-mail address: lc-guo@163.com (L. Guo).

0378-7753/$ – see front matter.
doi:10.1016/j.jpowsour.2011.06.104

practical use of IT-SOFCs, more convenient and economical methods should be exploited and used.

On the other hand, frit is widely used in preparing electrodes of electronic ceramics. The addition of frit to electrodes can effectively lower the sintering temperature and improve their sintering strength, especially for Ag, Cu or Al based electrodes.

This study aims to lower the sintering temperature of cathode-Ag by adding BBP frit. Attempts are made to investigate the effect of the Ag and BBP frit on the structure, thermal expansion, electrical conductivity and electrochemical performance of LBCO for IT-SOFCs cathode material.

2. Experimental

2.1. Powder synthesis

LBCO and SDC powders were synthesized by mechanical mixing method. La_2O_3, $BaCO_3$, Co_2O_3 and Sm_2O_3, CeO_2 were mixed in appropriate amount with an accuracy of ±0.1 mg according to the chemical compositions of LBCO and SDC, and then milled for 8 h in the distilled water by a planetary zirconia ball mill, respectively. The mixed powder LBCO was calcined at 1100 °C, but SDC at 1200 °C for 2 h in air for the complex oxides formation. The calcined SDC powder was milled again for 6 h. LBCO-*x*Ag powder was prepared by mixing as-prepared LBCO powder with appropriate amount of Ag_2O, and then milled for 8 h. After the evaporation of distilled water, the mixed powder was calcined at 900 °C for 3 h in air. The LBCO-*x*Ag_2O transformed to LBCO-*x*Ag on calcining at 900 °C.

In addition, a commercially available B_2O_3-Bi_2O_3-PbO frit (FSTC-550, Shockin Tech Nano Ceramic Ltd., Nanjing, China) was used in this study.

2.2. Sample preparation

The mixed powder of LBCO-*x*Ag with BBP frit (LBCO-*x*Ag-*y*BBP, *y* = 2.0, 2.5, 3.0, 3.5 wt.%) was pelletized (10–12 wt.% PVA was added) and then pressed at 10 MPa to form a bar using a Φ21.5 mm die. After calcined at 900 °C for 3 h, the bars were used to measure thermal expansion and electrical conductivity.

Pressed pellets of SDC were calcined at 1550 °C for 2 h in air. The powder consisting of LBCO-*x*Ag and BBP frit was mixed with ethyl cellulose and terpinol, and then painted symmetrically on both sides of the SDC pellets with the area of about 10 mm in diameter by screen painting method, followed by calcined at 900 °C for 3 h. The Ag paste as the reference electrode was painted onto the SDC surface with a ring shape about 3 mm away from the working electrode, and then calcined at 700 °C.

2.3. Characterization

The crystal structure and chemical compatibility were identified by XRD using the diffractometer with Cu Ka radiation (λ = 0.15418 nm). The diffraction angle 2θ was 20–80°. The microstructures of porous cathode and cross-sectional surface for composite cathode/electrolyte were characterized by scanning electron microscopy (SEM, JEOL, JSM-5900).

Thermal expansion was measured using a dilatometer (RPZ-01, Luoyang, China) in air from 50 °C to 800 °C at a heating rate of 5 °C min^{-1}. Electrical conductivity was measured using DC four-probe method from 200 °C to 800 °C at intervals of 50 °C in air.

Electrochemical impedance spectroscopy (EIS) and cathodic polarization analysis were performed using an electrochemical workstation (PARSTAT 2273). The impedance measurements were carried out on a symmetric cell with the configuration of cathode|electrolyte|cathode in the frequency range of 100 kHz to 0.1 Hz with ac voltage amplitude of 10 mV from 500 °C to 800 °C. Cathodic polarization analysis was tested on a three-electrode cell at 700 °C in air.

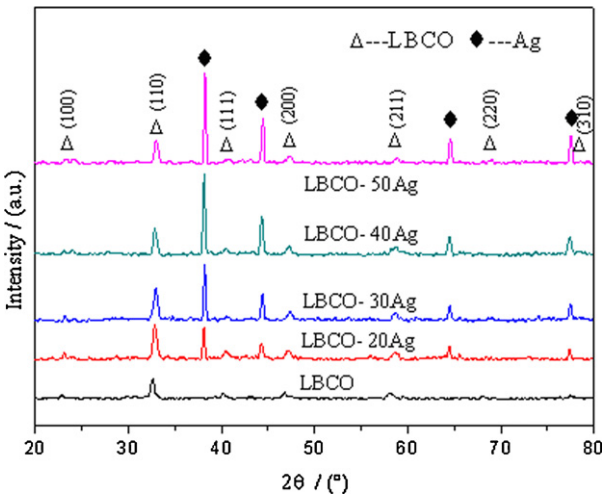

Fig. 1. XRD patterns of LBCO calcined at 1100 °C for 2 h and LBCO-*x*Ag cathodes calcined at 900 °C for 3 h.

3. Results and discussion

3.1. Crystal structure and chemical compatibility

The XRD pattern of LBCO calcined at 1100 °C for 2 h in air is shown in Fig. 1. It can be seen from the pattern that a pure-phase complex oxide of LBCO was identified without any detectable impurity phases. The same results were reported by Kim et al. [26], and Zhang et al. [27].

The mixed powders consisting of different amounts of LBCO and Ag were calcined at 900 °C for 3 h in air for the investigation of the chemical reaction between them. It was observed from the patterns of LBCO-*x*Ag in Fig. 1 that LBCO and Ag still remained their own structures and no additional peaks appeared, indicating that LBCO and Ag have good chemical compatibility. This makes Ag to function with its own advantages in the LBCO-*x*Ag composite cathodes. The results are similar to $Ba_{0.5}Sr_{0.5}Co_{0.8}Fe_{0.2}O_{3-\delta}$-$Sm_{0.2}Ce_{0.8}O_{1.9}$-Ag reported by Zhou et al. [28] and $La_{0.6}Sr_{0.4}Co_{0.2}Fe_{0.8}O_3$-$Sm_{0.1}Ce_{0.9}O_{1.95}$-Ag reported by Zhang et al. [18]. There was no Ag_2O phase identified for all the samples, proving that the LBCO-*x*Ag_2O transformed to LBCO-*x*Ag completely after calcining at 900 °C. In addition, the more the Ag content, the higher the peak of the LBCO-*x*Ag.

Fig. 2 shows the XRD patterns of LBCO-30Ag and LBCO-30Ag-2.5BBP calcined at 900 °C for 3 h. Contrast these two patterns, it can be seen that $Bi_4Pb_3O_{10}$, B_2O, $Ag_{99.5}Pb_{0.5}$ and $Ag_{99.5}Bi_{0.5}$ emerged, while the LBCO and Ag remained their own structures unchanged. The B_2O and Co_3O_4 phases may be related to the inhomogenous distribution of powders during the preparation process [29]. Several researchers [10,21] found that Ag-modified cathodes containing Bi ion showed better performance than pure cathode at the same condition, which indicate that the $Ag_{99.5}Bi_{0.5}$ will not negatively affect the performance of LBCO-Ag. The influence of all the new phases on the performance of LBCO-30Ag-2.5BBP cathode can be neglected because of their little content.

3.2. Microstructure

Fig. 3(a) and (b) show the microstructures of cross-section for LBCO-30Ag/SDC and LBCO-30Ag-2.5BBP/SDC, respectively, (c) and

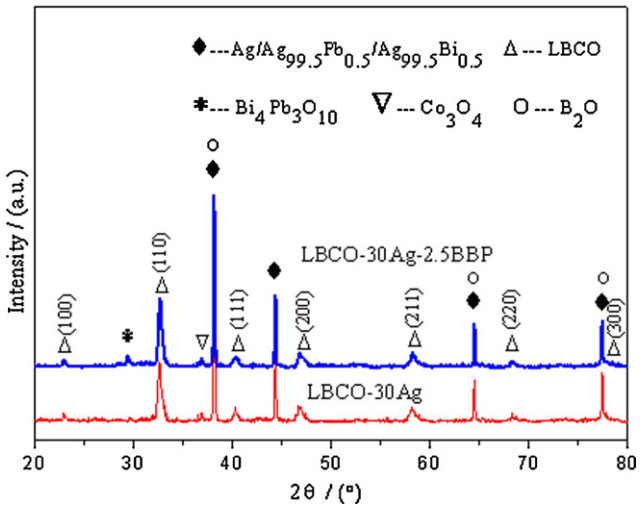

Fig. 2. XRD patterns of LBCO-30Ag and LBCO-30Ag-2.5BBP calcined at 900 °C for 3 h.

(d) show the porous cathode surface for LBCO-30Ag and LBCO-30Ag-2.5BBP calcined at 900 °C for 3 h in air.

The low sintering temperature of 900 °C resulted in only point contact among particles and a rather poor interfacial adhesion between LBCO-30Ag and SDC was observed in Fig. 3(a) and (c). However, an improved particles contact and an enhanced interfacial adhesion between LBCO-30Ag-2.5BBP and SDC was formed shown in Fig. 3(b) after the addition of appropriate amount of BBP, implying that the BBP frit can effectively enhance the sintering strength of LBCO-30Ag cathode. This phenomenon can be explained as follows. The low melting point of BBP frit makes the sintering of LBCO-30Ag-2.5BBP cathode a liquid phase sintering process. The BBP frit may accelerate the grain growth so that the LBCO-30Ag with BBP frit cathode can form a dense structure at a relative low sintering temperature (900 °C). For a uniform microstructure, a longer holding time (3 h) is needed, a sufficient time for the small grains dissolve in the liquid phase and other gains grow up.

Fig. 3(b) shows LBCO-30Ag-2.5BBP cathode calcined at 900 °C, thickness of the cathode functional layer was about 25 μm. The composite cathode LBCO-30Ag-2.5BBP was porous and had a reasonable porosity shown in Fig. 3(d), which benefits the transport of gas and facilitates the oxygen reduction reaction. We can conclude that the addition of appropriate amount of BBP frit to LBCO-*x*Ag can effectively improve the adhesion and strength of cathode membrane without damaging its porous structure.

3.3. Thermal expansion

Thermal expansion behavior was investigated to study the mechanical compatibility between the composite cathode and electrolyte. The thermal expansion of each part of SOFCs should match, otherwise may cause internal stress leading to crack of the material and affect the long-term stability of cell.

The thermal expansion curves of LBCO-*x*Ag-BBP (BBP frit was added to LBCO-*x*Ag at weight ratio of BBP:Ag = 1:12) in the temperature range of 50–800 °C are shown in Fig. 4. The thermal expansion increased with the elevated temperature. The thermal expansions of LBCO with various amounts of Ag and BBP were almost the same, indicating that the addition of Ag and BBP frit to LBCO had no significant effect on the thermal expansion.

The average thermal expansion coefficient (TEC) was calculated from the thermal expansion data. The average TECs of LBCO-*x*Ag-BBP are also listed in Fig. 4. Results indicate that the TECs of LBCO-*x*Ag-BBP were 16.6–16.9 × 10^{-6} K^{-1} over 50–800 °C, which

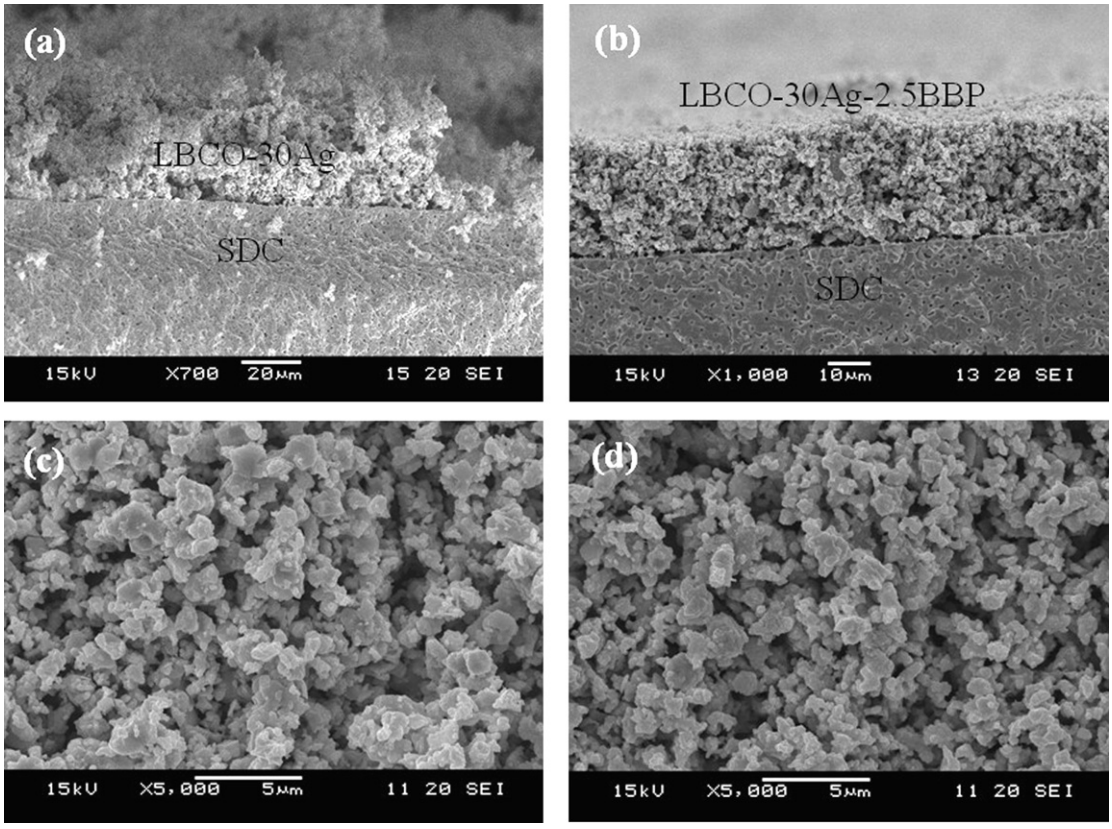

Fig. 3. SEM images of cross-section (a), surface (c) of LBCO-30Ag and cross-section (b), surface (d) of LBCO-30Ag-2.5BBP.

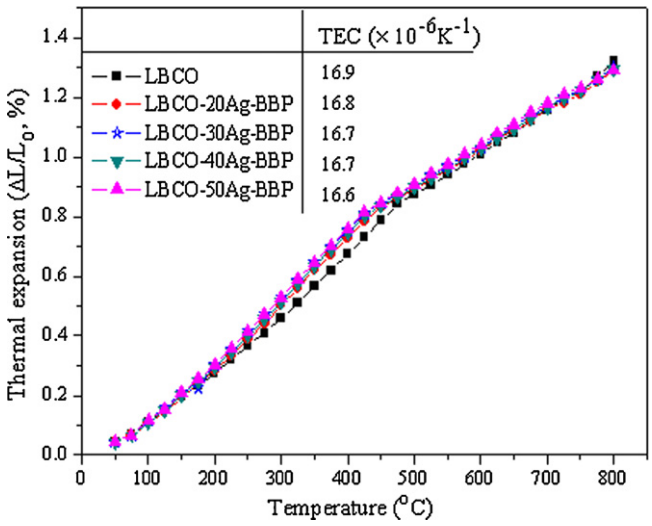

Fig. 4. Thermal expansion curves of LBCO-*x*Ag-BBP from 50 °C to 800 °C in air.

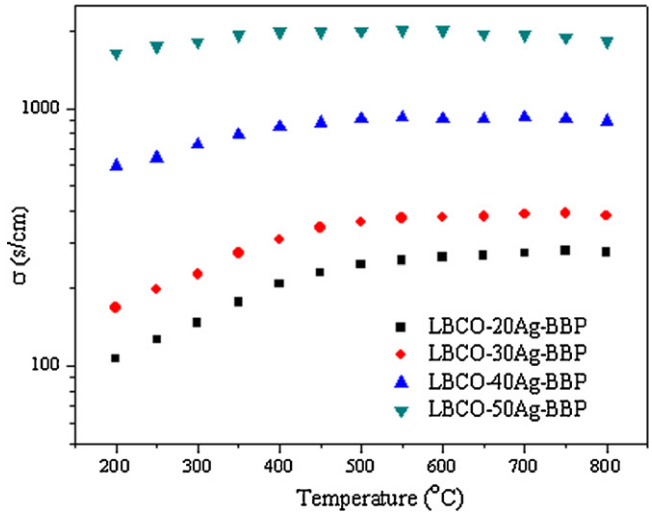

Fig. 5. Electrical conductivity of LBCO-*x*Ag-BBP from 200 °C to 800 °C in air.

are smaller than that of $LnBaCo_2O_{5+\delta}$ (Ln = La, Pr, Nd, Sm, Gd and Y) oxide reported by Kim et al. [26].

During our experiments, the LBCO-*x*Ag-BBP were applied as thin-layered (about 20–30 μm, seen in Fig. 3(b)) on the SDC electrolyte surface to minimize TEC mismatch between them.

3.4. Electrical conductivity

High electrical conductivity is a fundamental requirement for cathode materials. The electrical conductivity of LBCO-*x*Ag-BBP (BBP frit was added to LBCO-*x*Ag at weight ratio of BBP:Ag = 1:12) cathode as a function of temperature is shown in Fig. 5.

The electrical conductivity increased with increasing Ag content at the same temperature, which could be attributed to the high conductivity of Ag. For each sample, the electrical conductivity increased first and then decreased with increasing temperature, exhibiting a typical transition from semiconducting to metallic conducting behavior [5]. The decrease in electrical conductivity at higher temperature could be ascribed to the loss of lattice oxygen. In addition, with increasing Ag content, the metallic conducting behavior of LBCO-*x*Ag-BBP sample was more and more obvious after 500 °C. The electrical conductivity value of each sample was above 200 S cm^{-1} at 500–800 °C, satisfying the requirement for cathode material for IT-SOFCs.

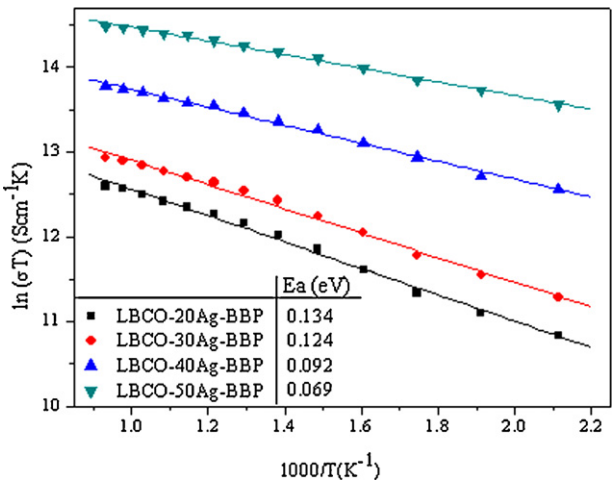

Fig. 6. Arrhenius plots of $\ln(\sigma T)$ vs. $1000\,T^{-1}$ for LBCO-*x*Ag-BBP.

The electrical conductivity was plotted as $\ln(\sigma T)$ versus $1000\,T^{-1}$ in Fig. 6. There was a linear relationship between $\ln(\sigma T)$ and $1000\,T^{-1}$ for all the samples, indicating that the conductivity behavior obeys the small polaron conductivity mechanism. The values of activation energy (Ea) calculated from the slope of the plots are also listed in Fig. 6. The Ea decreased with increasing Ag content over 200–800 °C. According to Lee et al. [30], the Ea has a close relationship with the polaron binding energy (Ep) and bandwidth (*W*). The decrease in activation energy with increasing Ag content may be ascribed to the decrease in Ep or the increase in *W*.

3.5. Electrochemical impedance spectroscopy

The impedance spectra was fitted through a fitting software (ZSimpwin) by an equivalent circuit with a configuration of $LR_{ohm}(Q_1R_1)(Q_2R_2)$. *L* is the high-frequency inductance, corresponding to the arc below the real axis. R_{ohm} is the overall ohmic resistances including the electrolyte resistances, electrodes resistances, lead wires resistances and touch resistances, which corresponds to the left of the high frequency intercept [31]. According to the analysis process, all the impedance spectra could be separated into two arcs (the high frequency arc and the low frequency arc), indicating that the oxygen reduction reaction could be composed of at least two different processes: the charge transfer process and diffusion process (including the oxygen adsorption or desorption on the electrode surface and diffusion of oxygen ions) [28,32]. R_1 and R_2 are the electrode polarization resistances at high and low frequencies, respectively. Q_1 and Q_2 are the corresponding constant phase elements.

The total electrode polarization resistance Rp is the sum of R_1 and R_2, which is the difference between real axes intercepts of the impedance spectra. The ohmic resistance R_{ohm} of each sample was subtracted in order to compare the Rp of different cathodes directly during our experiments.

3.5.1. Effect of Ag content on polarization resistance

Impedance spectra of LBCO-*x*Ag-BBP (BBP frit was added to LBCO-*x*Ag at a weight ratio of BBP:Ag = 1:12) cathode based on SDC electrolyte under open circuit potential at 700 °C is shown in Fig. 7.

It can be seen from Fig. 7 that the Rp of LBCO-*x*Ag-BBP decreased first and then increased with increasing Ag content, reaching a minimum at 30 wt.% Ag. The initial decreased in the Rp was related

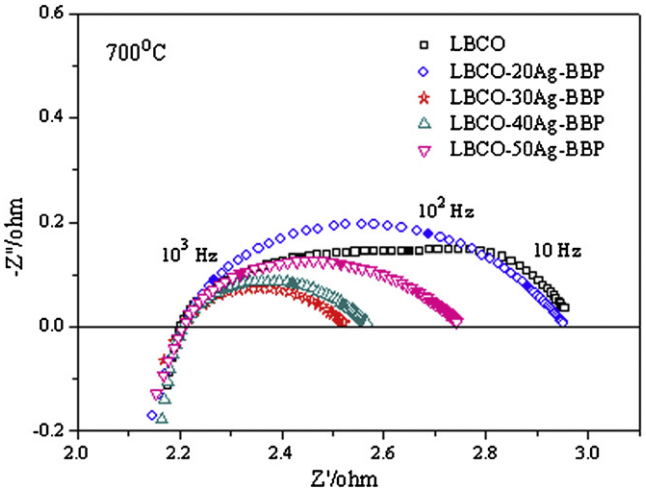

Fig. 7. Impedance spectra of LBCO-*x*Ag-BBP cathodes at 700 °C under open circuit potential in air.

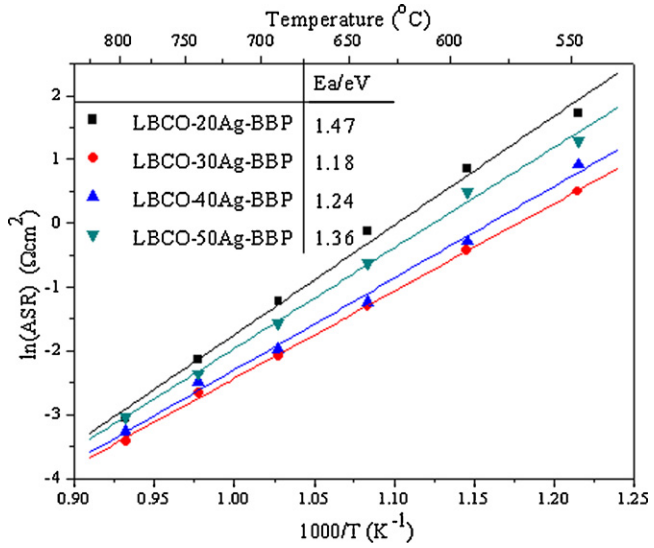

Fig. 8. Arrhenius plots of ASRs for LBCO-*x*Ag-BBP cathodes at 550–800 °C.

to the increase in the electronic conductivity and catalytic activity contributed by Ag. However, when Ag content >30 wt.%, the excessive Ag particle leads to the smaller active sites for ORR and the continuous paths of the oxide ion may be interrupted, leading to the increase in Rp. The similar result has been reported by several researchers [8,20,21].

For each sample, the low frequency (<10^3 Hz) resistance R_2 was larger than high frequency resistance R_1. This indicated that the R_2 related process (the diffusion process) probably limited the ORR rate. R_2 decreased significantly with increasing temperature, implying that the diffusion process was enhanced by increasing temperature.

For LBCO-*x*Ag-BBP, the R_2 were much smaller than that of LBCO, which implied that the diffusion process was enhanced significantly by the addition of Ag.

The Rp of the single electrode is half that of the obtained polarization resistance because the two-electrode configuration was used during our experiments. Therefore, the area specific resistance (ASR) can be deduced from the following equation:

$$\mathrm{ASR} = \frac{R_\mathrm{P} \times \text{electrode area}}{2} \quad (1)$$

The ASR values of LBCO-*x*Ag-BBP composite cathodes at 550–800 °C are shown in Table 1. For all the samples, the ASR decreased with the elevated temperature. It can be seen that the LBCO-30Ag-BBP cathode exhibited the lower ASR than other samples at the corresponding temperature. The lowest ASR was 0.033 Ω cm^2 obtained when the Ag content reached 30 wt.% at 800 °C, which was much lower than that of single LBCO cathode (0.137 Ω cm^2). In addition, the ASR of LBCO-30Ag-BBP at 700 °C (0.125 Ω cm^2) is much smaller than that of pure Ag electrode on SDC electrolyte (3.9 Ω cm^2, reported by Huang et al. [33]).

The ASR of LBCO-30Ag-BBP was 0.271 Ω cm^2 at 650 °C and 0.070 Ω cm^2 at 750 °C, the former is smaller than that of $(BaO)_{0.11}(Bi_2O_3)_{0.89}$-50 vol.% Ag prepared by ball milling [21] and the latter is equal to that of $Ba_{0.5}Sr_{0.5}Co_{0.8}Fe_{0.2}O_{3-\delta}$-3 wt.% Ag prepared by the impregnation method at the same temperature [22]. It is evident that the LBCO-30Ag-BBP cathode may be a potential cathode for IT-SOFCs.

The Arrhenius plots of the ASR for LBCO-*x*Ag-BBP cathodes at various temperature are shown in Fig. 8, and the values of activation energy (Ea) calculated from the slope of the plots are also listed. It is obviously that there was a linear relationship between ln(ASR) and 1000 T^{-1} for all the four samples, indicating that a constant Ea was obtained for each sample. The LBCO-30Ag-BBP showed the lowest Ea of 1.18 eV (~114 kJ mol^{-1}), indicating that the addition of 30 wt.% Ag to LBCO decrease the Ea and increase the ORR activity more significantly than other samples in the experiment range. The Ea of different composite cathodes were similar in magnitude, indicating that the reaction mechanism is similar among these cathodes based on SDC electrolyte [29].

3.5.2. *Effect of BBP frit content on polarization resistance*

The impedance spectra of LBCO-30Ag-*y*BBP (*y* = 2.0, 2.5, 3.0, 3.5 wt.%) cathodes were investigated to study the effect of BBP frit content on the properties of LBCO-30Ag composite cathodes. Fig. 9 shows the impedance spectra of LBCO-30Ag-*y*BBP based on SDC electrolyte at 700 °C, 750 °C and 800 °C.

The Rp decreased as BBP frit content increased up to 2.5 wt.% and further increasing BBP frit content caused an increase of Rp at the same temperature. This tendency can be found at each temperature. The Rp value has a close relationship with the microstructure of composite cathode with BBP frit. When the BBP frit content is <2.5 wt.%, the composite cathodes LBCO-30Ag-*y*BBP are difficult to form a dense structure and the interfacial adhesion between composite cathode and electrolyte is rather poor after sintering. It is impossible to form the relatively dense cathode functional layer. The composite cathode LBCO-30Ag-2.5BBP calcined at 900 °C has a structure with reasonable porosity and shows good adhesion to SDC electrolyte (seen in Fig. 3(b)), exhibiting the best performance. However, when the BBP frit content more than 2.5 wt.%, the excessive BBP could destroy the porous structure of composite cathode and form a too dense structure, which is not beneficial for the transport of the oxygen ion and gas, leading to a decreased cathode performance. In addition, the content of $Bi_4Pb_3O_{10}$, $Ag_{99.5}Pb_{0.5}$ and $Ag_{99.5}Bi_{0.5}$ phases (seen in Fig. 2) will increase with increasing BBP frit content, which not only occupy the active sites for ORR, but also interrupt the continuous paths of the oxide ion.

For LBCO-30Ag-*y*BBP, the R_1 were larger than that of LBCO, but the R_2 were much smaller than that of LBCO, which implied that the BBP frit mainly improves the diffusion process but hinders the charge transfer process. The difference between R_1 and R_2 became smaller with increasing temperature, indicating that the diffusion process is more active at higher temperature.

Table 1
ASR values of LBCO-*x*Ag-BBP cathodes at 550–800 °C.

T (°C)	Area-specific resistance (ASR) (Ω cm^2)				
	LBCO	LBCO-20Ag-BBP	LBCO-30Ag-BBP	LBCO-40Ag-BBP	LBCO-50Ag-BBP
550	2.321	5.642	1.643	2.501	3.670
600	1.034	2.353	0.655	0.750	1.634
650	0.566	0.875	0.271	0.291	0.533
700	0.295	0.293	0.125	0.140	0.210
750	0.177	0.119	0.070	0.083	0.095
800	0.137	0.047	0.033	0.038	0.048

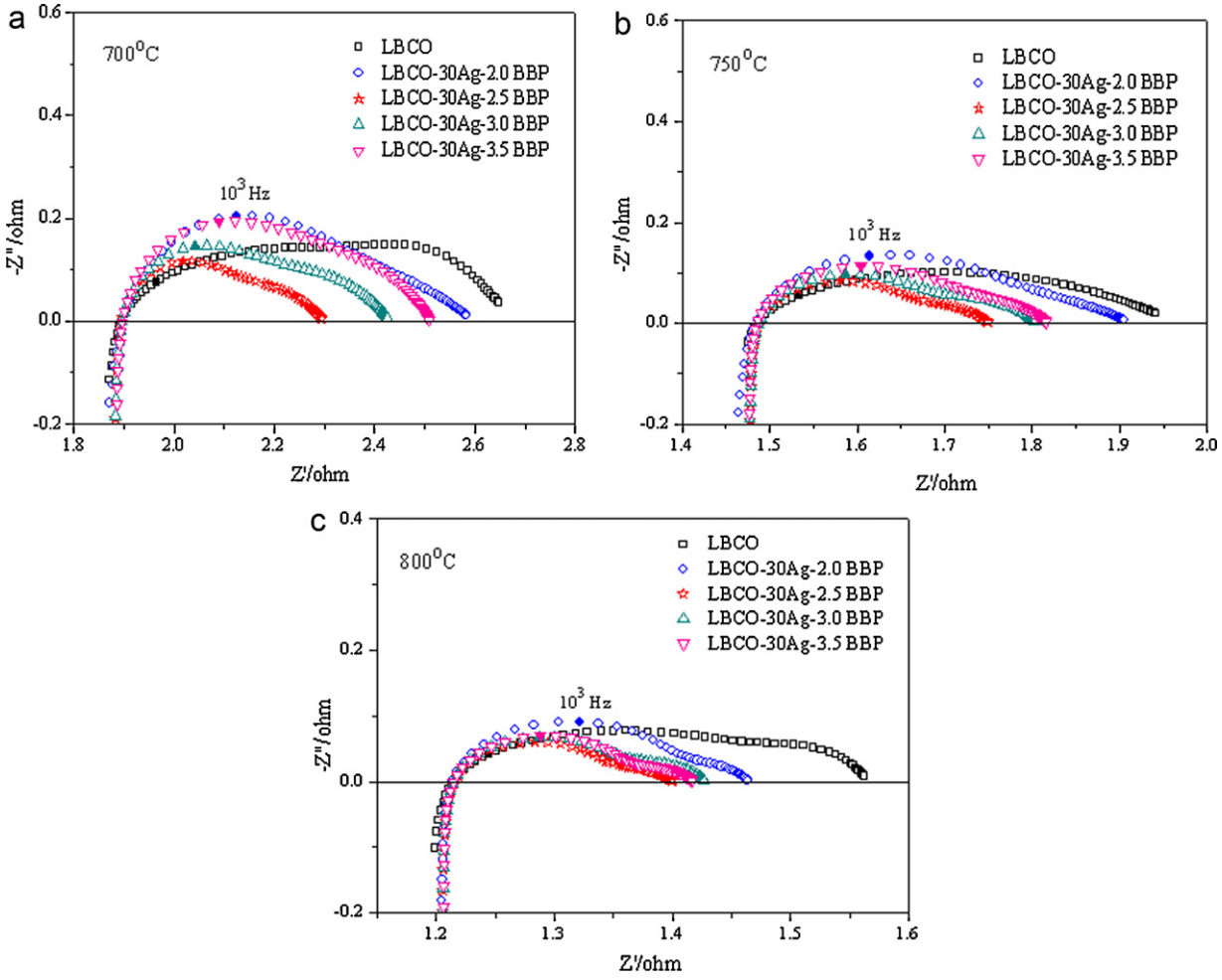

Fig. 9. Impedance spectra of LBCO-30Ag-*y*BBP cathodes at 700 °C (a), 750 °C (b) and 800 °C (c) under open circuit potential in air.

3.6. Cathodic polarization analysis

The cathodic overpotential is an important factor to evaluate the cathode performance. It is well known that the lower overpotential of cathode implying a better stability of cathode and a higher electrocatalytic activity for ORR.

3.6.1. Effect of Ag content on polarization overpotential

The overpotential of LBCO-*x*Ag-BBP (BBP frit was added to LBCO–*x*Ag at weight ratio of BBP: Ag = 1:12) cathodes based on SDC electrolyte at 700 °C are shown in Fig. 10. It can be seen that the overpotential decreased first and then increased with increasing Ag content at the same current density. The tendency is consistent with the result of the EIS in Fig. 7. Obviously, the cathodic overpotential were 31.0 mV, 10.7 mV, 13.2 mV and 37.5 mV for LBCO-*x*Ag-BBP (x = 20, 30, 40, 50) at a current density of 0.2 A cm^2 at 700 °C, respectively, while the value was 51.0 mV for LBCO in the same condition.

3.6.2. Effect of BBP frit content on polarization overpotential

Fig. 11 shows the overpotential of LBCO-30Ag-*y*BBP cathodes based on SDC electrolyte at 700 °C. When the frit content reached 2.5 wt.%, the lowest polarization overpotential was obtained and then increased above that. The tendency is in agreement with the previous EIS result in Fig. 9. It is reasonable to expect that the electrochemical activity of LBCO cathode could be further improved by the addition of appropriate amount of Ag and BBP frit.

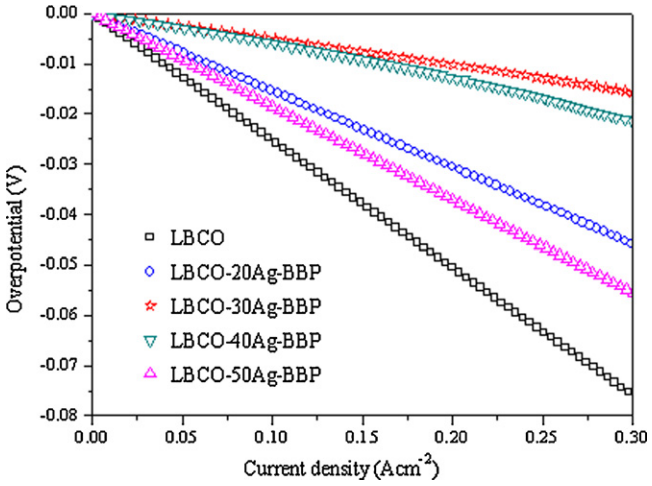

Fig. 10. Polarization curves for LBCO-*x*Ag-BBP cathodes at 700 °C in air.

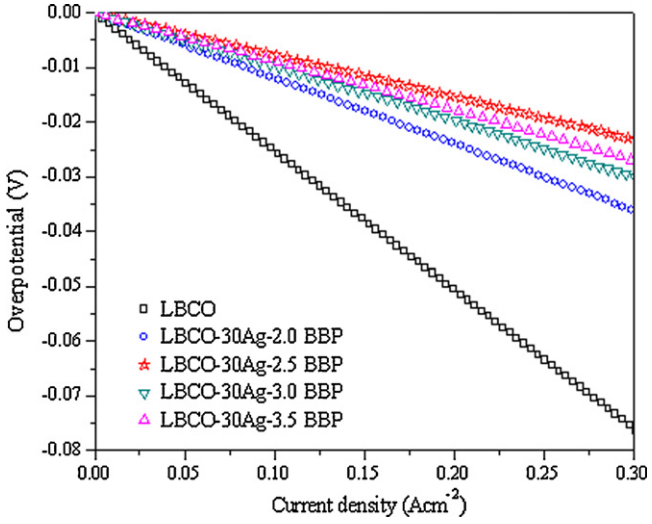

Fig. 11. Polarization curves for LBCO-30Ag-*y*BBP cathodes at 700 °C in air.

4. Conclusions

This study focused on lowering the sintering temperature and improving the sintering strength of LBCO-*x*Ag composite cathode to 900 °C by adding a small amount of BBP frit. According to SEM images, BBP frit can effectively improve the adhesion and strength of cathode membrane without damaging its porous structure. The XRD patterns showed that the LBCO calcined at 1100 °C for 2 h obtained as a single perovskite-related oxide phase and had good chemical compatibility with Ag and BBP, but there existed a slight reaction between Ag and BBP. The electrical conductivity of LBCO-*x*Ag-BBP increased as the Ag content increased. Ag and BBP frit played important roles in improving the electrochemical performance of LBCO. The ASR and cathodic overpotential of LBCO-*x*Ag-BBP decreased first and then increased with increasing Ag content, reaching minimum values of 0.033 Ω cm^2 at 800 °C (0.070 Ω cm^2 at 750 °C, 0.125 Ω cm^2 at 700 °C) and 10.7 mV at a current density of 0.2 A cm^{-2} at 700 °C around $x = 30$. The optimal BBP frit content in LBCO-30Ag-BBP composite cathodes was 2.5 wt.%. The LBCO-30Ag-2.5BBP composite cathode may be a potential high performance cathode for IT-SOFCs.

In addition, the polarization resistance Rp of LBCO-30Ag-2.5BBP in Fig. 7 (BBP was added to LBCO-*x*Ag at weight ratio of BBP:Ag = 1:12, that is, the BBP content in LBCO-30Ag is 2.5%) and Fig. 9 should be the same at the corresponding temperature in theory. However, there exists minor difference between them during our experiments, which may be attributed mostly to the staring materials of Co_2O_3 used in these two processes were bought from different manufacturers.

Acknowledgements

This research was financially supported by the Commercialization of Scientific and Technological Achievements Program of Jiangsu Province (BE2009169). We also acknowledge the support of A Project Funded by the Priority Academic Program Development of Jiangsu Higher Education Institutions (PAPD).

References

[1] N.Q. Minh, J. Am. Ceram. Soc. 76 (1993) 563–588.
[2] J. Molenda, K. Świerczek, W. Zając, J. Power Sources 173 (2007) 657–670.
[3] V. Verda, M.C. Quaglia, Int. J. Hydrogen Energy 33 (2008) 2087–2096.
[4] C. Gaudillère, L. Olivier, P. Vernoux, C. Zhang, Z. Shao, D. Farrusseng, J. Power Sources 195 (2010) 4758–4764.
[5] X. Ding, C. Cui, X. Du, L. Guo, J. Alloys Compd. 475 (2009) 418–421.
[6] A. Tarancón, A. Morata, G. Dezanneau, S.J. Skinner, J.A. Kilner, S. Estradé, F. Hernández-Ramírez, F. Peiró, J.R. Morante, J. Power Sources 174 (2007) 255–263.
[7] Q. Zhou, F. Wang, Y. Shen, T. He, J. Power Sources 195 (2010) 2174–2181.
[8] K.T. Lee, A. Manthiram, J. Power Sources 160 (2006) 903–908.
[9] K. Sasaki, J. Tamura, M. Dokiya, Solid State Ionics 144 (2001) 233–240.
[10] Z. Gao, Z. Mao, J. Huang, R. Gao, C. Wang, Z. Liu, Mater. Chem. Phys. 108 (2008) 290–295.
[11] K. Sasaki, J. Tamura, H. Hosoda, T.N. Lan, K. Yasumoto, M. Dokiya, Solid State Ionics 148 (2002) 551–555.
[12] T.Z. Sholklapper, V. Radmilovic, C.P. Jacobson, S.J. Visco, L.C. De Jonghe, J. Power Sources 175 (2008) 206–210.
[13] M. Sahibzada, S.J. Benson, R.A. Rudkin, J.A. Kilner, Solid State Ionics 113–115 (1998) 285–290.
[14] Y. Liu, M. Mori, Y. Funahashi, Y. Fujishiro, A. Hirano, Electrochem. Commun. 9 (2007) 1918–1923.
[15] T. Huang, X. Shen, C. Chou, J. Power Sources 187 (2009) 348–355.
[16] V.A.C. Haanappel, D. Rutenbeck, A. Mai, S. Uhlenbruck, D. Sebold, H. Wesemeyer, B. Röwekamp, C. Tropartz, F. Tietz, J. Power Sources 130 (2004) 119–128.
[17] Y. Sakito, A. Hirano, N. Imanishi, Y. Takeda, O. Yamamoto, Y. Liu, J. Power Sources 182 (2008) 476–481.
[18] J. Zhang, Y. Ji, H. Gao, T. He, J. Liu, J. Alloys Compd. 395 (2005) 322–325.
[19] S. Uhlenbruck, F. Tietz, V. Haanappel, D. Sebold, H.P. Buchkremer, D. Stöver, J. Solid State Electrochem. 8 (2004) 923–927.
[20] W. Zhou, R. Ran, Z. Shao, R. Cai, W. Jin, N. Xu, J. Ahn, Electrochim. Acta 53 (2008) 4370–4380.
[21] S. Huang, Z. Zong, C. Peng, J. Power Sources 173 (2007) 415–419.
[22] Y. Lin, R. Ran, Z. Shao, Int. J. Hydrogen Energy 35 (2010) 8281–8288.
[23] Z.G. Lu, J.H. Zhu, Electrochem. Solid-State Lett. 10 (10) (2007) B179–B182.
[24] S. Huang, Z. Wen, J. Zhang, X. Yang, Electrochim. Acta 52 (2007) 3704–3708.
[25] W. Zhou, R. Ran, R. Cai, Z. Shao, W. Jin, N. Xu, J. Power Sources 186 (2009) 244–251.
[26] J.H. Kim, A. Manthiram, J. Electrochem. Soc. 155 (4) (2008) B385–B390.
[27] K. Zhang, L. Ge, R. Ran, Z. Shao, S. Liu, Acta Mater. 56 (2008) 4876–4889.
[28] W. Zhou, Z. Shao, R. Ran, Z. Chen, P. Zeng, H. Gu, W. Jin, N. Xu, Electrochim. Acta 52 (2007) 6297–6303.
[29] X. Ding, L. Gao, Y. Liu, Y. Zhen, L. Guo, J. Electroceram. 18 (2007) 317–322.
[30] K.T. Lee, A. Manthiram, J. Electrochem. Soc. 152 (1) (2005) A197–A204.
[31] H. Gu, H. Chen, L. Gao, L. Guo, Electrochim. Acta 54 (2009) 7094–7098.
[32] Y. Cao, H. Gu, H. Chen, Y. Zheng, M. Zhou, L. Guo, Int. J. Hydrogen Energy 35 (2010) 5594–5600.
[33] S. Huang, G. Zhou, Y. Xie, J. Alloys Compd. 464 (2008) 322–326.